Available online at www.sciencedirect.com
SCIENCE DIRECT®
ELSEVIER
Ultramicroscopy 97 (2003) 145–150
ultramicroscopy
www.elsevier.com/locate/ultramic

In-plane contributions to phase contrast in intermittent contact atomic force microscopy

Matthew S. Marcus[a], M.A. Eriksson[a,*], Darryl Y. Sasaki[b], Robert W. Carpick[c]

[a] *Physics Department, University of Wisconsin-Madison, Madison, WI, USA*
[b] *Sandia National Laboratories, Biomolecular Materials and Interface Science Department, Albuquerque, NM, USA*
[c] *Department of Engineering Physics, Materials Science Program, and Rheology Research Center, University of Wisconsin-Madison, Madison, WI, USA*

Received 28 June 2002; received in revised form 14 October 2002

Abstract

Contrast in the phase response of intermittent-contact atomic force microscopy (IC-AFM) reveals in-plane structural and mechanical properties of polymer monolayers. This result is unexpected, as IC-AFM has previously only been considered as a probe of out-of-plane properties. Until now, AFM measurements of nanoscale in-plane properties have employed contact mode techniques. In-plane property measurements are possible with intermittent contact AFM because there is a small but significant component of tip motion parallel to the sample surface. This in-plane component of tip displacement is virtually universal in AFM, implying that oscillating-tip techniques generally are sensitive to in-plane material properties. We present a simple Hertzian model of intermittent-contact AFM that includes such an in-plane displacement.

PACS: 68.47.Pe; 68.35.Af; 07.79.Sp; 68.37.Ps

Keywords: AFM

1. Introduction

Anisotropic properties are common in a wide variety of materials. Strong three-dimensional anisotropies are common in layered materials, such as many minerals [1] and biological structures such as Abalone shells [2]. Friction at the nanoscale can also be anisotropic, and this has many origins, including the tilting of molecular groups with respect to the surface normal, as in lipid monolayers [3], the relative crystallographic orientation between monolayer structures and substrates [4], and well-defined polymer chain features in monolayer films [5,6]. Such anisotropic surfaces are of interest for applications including nanofabrication and nanomanipulation [4].

The tips of scanning probe microscopes frequently are rotationally symmetric, with no good reference from which to measure a surface anisotropy. Nonetheless, anisotropies at nanometer length scales have been measured using a variety of scanning probe techniques [3,4,7–10]. In such

*Corresponding author.
E-mail address: maeriksson@facstaff.wisc.edu (M.A. Eriksson).

0304-3991/03/$ - see front matter
doi:10.1016/S0304-3991(03)00039-1

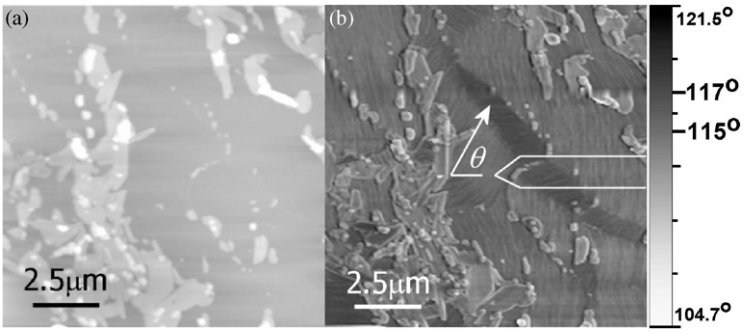

Fig. 1. Topographic (a) and phase (b) images of a PDA monolayer thin film on mica. θ is the angle between the local PDA backbone striations and the long axis of the cantilever.

measurements, the tip–sample rotational symmetry is broken by a variety of methods. For example, in LFM the raster scan direction breaks this symmetry and provides the reference direction for measurements of frictional forces.

In this paper, we demonstrate that the cantilever tilt in intermittent-contact atomic force microscopy (IC-AFM) breaks the tip–sample rotational symmetry and enables measurements of in-plane anisotropic forces. The anisotropic forces result in varying energy dissipation depending on the cantilever-sample orientation, yielding phase contrast. The samples we use are poly(diacetylene) (PDA) monolayers on mica substrates. We observe phase differences of order 2°, corresponding to approximately 2.4 eV per cycle differences in energy dissipation between domains. We present a simple model of IC-AFM that explicitly includes a tilted cantilever.

2. Results and discussion

PDA monolayer films were prepared on a mica substrate using a Langmuir deposition technique [6]. PDA monolayers exhibit strong anisotropy that is correlated with their aligned polymer backbone structure [5,6,11,12]. For example, frictional forces measured with LFM on PDA monolayers are three times larger when sliding perpendicular vs. parallel to these backbones [5,6,11,12], an effect that is likely due to anisotropy in the monolayer's inelastic shear deformation modes [5].

Fig. 1(a) shows an IC-AFM topographic image of a PDA film with large monolayer regions [13]. The image was acquired with a Digital Instruments Multimode SPM and Nanoscope IIIa controller, using Si cantilevers in ambient laboratory conditions. Experimental parameters are listed in Table 1. Islands of multilayer PDA are also visible. The monolayer regions are polycrystalline, and each domain can be identified by the orientation of the striations visible in the phase image along which the PDA backbones lie [6,14]. The typical phase ϕ in Fig. 1(b) is approximately 116°.[1] Surprisingly, the phase ϕ differs from domain to domain by up to 2° in Fig. 1(b). The maximum phase ϕ_{max} occurs when the long axis of the cantilever is parallel to the striations ($\theta = 0°$).

Phase shifts in IC-AFM indicate energy loss [15]. When the tip's motion is sinusoidal, the power dissipated due to the tip–sample interaction is [15,16]:

$$\tilde{P}_{tip} = \frac{1}{2}\frac{kA^2\omega_0}{Q}\left(\frac{A_0}{A}\sin(\phi) - 1\right), \quad (1)$$

where ϕ is the phase of the oscillation relative to the drive, and the other parameters are in Table 1. We show below that, consistent with many IC-AFM measurements, the tip motion is very nearly sinusoidal in our experiments.

Fig. 2 shows the power dissipated from Fig. 1(b), as determined by Eq. (1). Fig. 2 shows that the power dissipated is smallest when the

[1] The reported phase shifts are true phase shifts with respect to the drive signal. The phase shifts reported by the instrument are not properly scaled and are shifted by 90°.

Table 1

Cantilever spring constant[a]	$k \sim 60$ N/m
Resonance frequency	$f_0 = 271$ kHz
Quality factor	$Q = 560$
Free amplitude	$A_0 = 10.5$ nm
Damped amplitude	$A = 7.7$ nm
Tip radius[a]	$R \sim 20$ nm
Cantilever width	$W = 125$ μm
Cantilever thickness	$T = 4$ μm
Cantilever tip height	$H = 12.5$ μm
Reduced contact modulus	$K = 10.5$ GPa

[a] Estimates based on the mean value reported by the manufacturer.

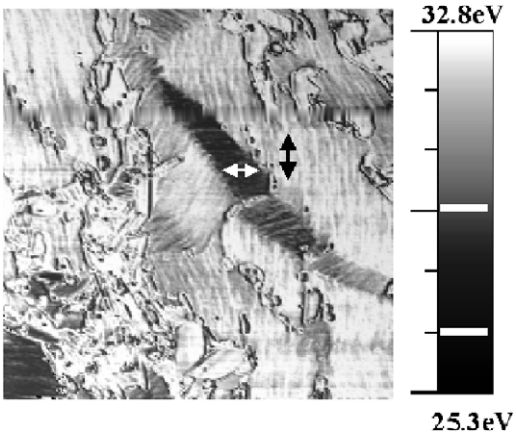

Fig. 2. The data from Fig. 1(b), plotted as energy loss via Eq. (1).

striations are parallel to the long axis of the cantilever. In fact, the cantilever loses an extra amount of energy $\Delta E \approx 2.4$ eV per cycle in domains where the striations are perpendicular, rather than parallel to the long axis of the cantilever. This amount of energy is roughly 10% of the total energy dissipated through the tip–sample interaction. That this level of energy loss should occur due to in-plane forces is not surprising, given that the tip moves in the plane of the sample a distance that is $\sim 20\%$ of the total tip displacement.

A simple model for an in-plane anisotropic tip–sample interaction force $F_{\text{in-plane}}$ is an isotropic dissipative force F_1, plus an anisotropic term that varies as $\sin(\theta)$ with maximum value F_2:

$$F_{\text{in-plane}} = F_1 + F_2|\sin(\theta)|, \tag{2}$$

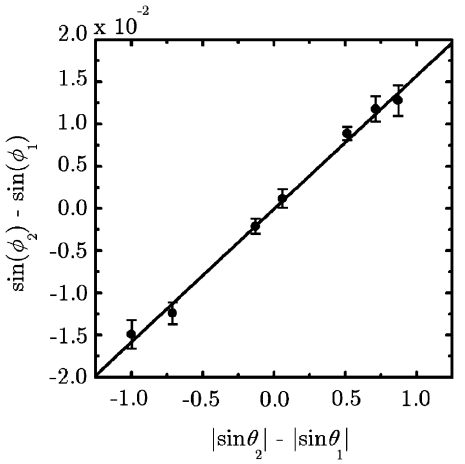

Fig. 3. The difference in the sines of the phase angles ϕ, proportional to the difference in energy loss between domains, versus the difference in the absolute values of the sines of the angles θ, proportional to the difference in the in-plane tip–sample dissipative forces. The line is $\Delta\sin(\phi) = \alpha\,\Delta\sin(\theta)$ with $\alpha = (1.58 \pm 0.05) \times 10^{-2}$.

where θ is defined in Fig. 1(b). Eq. (2) accurately describes the anisotropic friction force between PDA monolayers and LFM tips [5], where it was found that $F_2 \approx 2F_1$.

Fig. 3 is a plot of $\Delta\sin(\phi)$ vs. $\Delta|\sin(\theta)|$for the data in Fig. 1 [13]. Remarkably, we find that $\Delta\sin(\phi)$ is proportional to $\Delta|\sin(\theta)|$, with proportionality constant $\alpha = (1.58 \pm 0.05) \times 10^{-2}$. This linear proportionality is discussed in detail in Ref. [13]. If Eq. (2) describes the power dissipation, then the observed proportionality can be understood. In this case, the difference in $F_{\text{in-plane}}$ between two domains is simply proportional to $\Delta|\sin(\theta)| \equiv |\sin(\theta_2)| - |\sin(\theta_1)|$. The difference in power dissipated between two domains is proportional to $\Delta\sin(\phi) \equiv \sin(\phi_2) - \sin(\phi_1)$, from Eq. (1).

The anisotropic forces in our experiment most likely arise from two sources: friction and inelastic shear deformation. In fact, both effects must be present. Because the tip is moving at a finite lateral velocity with respect to the sample just before contact, there will initially be relative motion between the tip and sample as the tip does work on the surface to increase the surface lateral velocity to match that of the tip. Similarly, as the

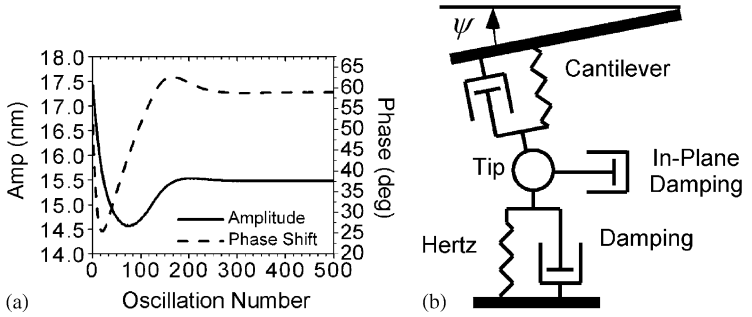

Fig. 4. Peak-to-peak amplitude (solid) and phase (dashed) data from a numerical simulation solving Eq. (3) for 500 oscillations. Transients in the signal diminish to yield a steady-state solution (constant amplitude and phase) after ~300 oscillations. Simulation parameters $K = 10.47\,\mathrm{GPa}$, $k = 60\,\mathrm{N/m}$, $A_0 = 10.5\,\mathrm{nm}$, $M = 40$, $Q_c = 4$.

tip slows and reverses direction near maximum compression into the sample, at some point its lateral velocity will match that of the surface. Any degree of static friction will then require a finite shear deformation before any relative sliding resumes [17]. Friction and shear deformation are closely related on the length scales considered here [18]. If the sample response is inelastic, then this shear deformation will also contribute to energy dissipation.

Although phase shifts arise from energy loss, variations in *elastic* forces can still result in variations in phase shift in an image. Such an effect could arise, for example, if in-plane elastic forces altered the overall motion of the tip. Although this effect is certainly present at some level in our measurements, we have previously shown that a very large elastic anisotropy would be required to account for the observed data in Fig. 1 [13].

There are a number of previous models which address the mechanism of IC-AFM [19–24]. These models are important as they relate various properties including adhesion, van der Waals' forces, elasticity, and material damping to the measured response. However, these models all assume that the tip's motion is purely normal to the sample surface. Fig. 4(b) is a schematic of a simple dynamic model of IC-AFM designed to explain the essential characteristics of our results. The critical feature is that the tip is constrained to move along the z'-axis, which is tilted an angle $\psi = 11^\circ$ from the sample normal. To solve for the motion of the tip, all tip–sample forces are projected onto the z'-axis. Ignoring motion along x' is a good approximation, as an analysis of the cantilever indicates that the effective spring constant in the x'-direction is more than 30 times larger than any other spring constant in the model [25].

The key result of this model is that the sample compression during contact now occurs along z', resulting in components of motion in both z- and the x-directions, Fig. 4(b). The in-plane motion along x is what we have demonstrated here. The forces on the tip are: (i) the cantilever restoring force and a damping force due primarily to interactions with the air, both acting along the z'-direction; (ii) a Hertz contact force acting in the z-direction; (iii) tip–sample damping along the z-direction acting during contact, due to inelastic deformation along z, taken to be larger than the air damping by a typical factor $M = 40$ [19]; and (iv) a viscous tip–sample interaction along x during contact, incorporating dissipative forces due to both shear deformation and friction. The cantilever is driven at its resonance frequency ω_0, giving:

$$\ddot{p} + \frac{\omega_0}{Q}(\dot{p} - \dot{\zeta}) + \omega_0^2(p - \zeta) = \begin{cases} 0 & p < 0, \\ -\frac{\omega_0^2}{k}\left(\cos^{5/2}(\psi) K \sqrt{R} p^{3/2} + \frac{Mk\cos^2(\psi)}{Q\omega_0}\dot{p} + \frac{k\sin^2(\psi)}{Q_c\omega_0}\dot{p}\right) & p \geqslant 0, \end{cases} \tag{3}$$

where p is the distance between the tip and sample along z', defined to be zero when the tip first touches the sample and positive when in contact. The displacement of the fixed end of the

cantilever z drives the cantilever on resonance: $\zeta = \zeta_0 + (A_0/Q)\sin(\omega_0 t)$. K is the reduced contact modulus, k is the cantilever force constant, R is the tip radius, Q is the damping due to air, and Q_c is the in-plane damping. The typical output from the model is shown in Fig. 4.

Using parameters appropriate for Fig. 1 (see Table 1) we solve for the steady-state motion of the tip. The model indicates a maximum tip–sample compression of 0.27 nm along z', giving a tip–sample in-plane tip motion of $\delta = 49.9 \pm 0.1$ pm along the x-direction. The time spent in contact with the surface is 0.35 μs/cycle. The distance δ is extremely small, and it is difficult to make firm distinctions between friction and shear deformation at such a small scale. The important result of the calculation is that the distance δ is virtually independent of the in-plane damping. Furthermore, our model produces a nearly sinusoidal tip motion, indicating that Eq. (1) remains valid for the tilted-cantilever geometry.

There are several models of IC-AFM [15,19–22,26–30], many of which include sophisticated treatments of adhesion and viscoelasticity—effects we have either ignored or simplified in our model. The distinguishing feature we have introduced is that the tip oscillates along an off-normal line. It is this feature that breaks the rotational symmetry of the tip–sample interaction and explains the behavior shown in Figs. 1–3.

The phase shifts ϕ in Fig. 1(b) differ from domain-to-domain, but they are constant within each domain. In principle, we can use our model to quantitatively associate the measured phase shifts with the dissipative in-plane properties of the material being imaged. These contributions are friction (as quantified by the interfacial shear strength τ between the tip and sample) [12] and dissipative shear deformation (due to viscoelasticity of the sample, as quantified by the loss tangent of the material, $\tan\Delta$) [31]. However, as discussed above, both of these mechanisms contribute to the observed dissipation and so we cannot explicitly separate them in our data. However, we can use our data to determine the upper limits of τ and $\tan\Delta$ by finding the values that result when attributing all the dissipation to each mechanism, respectively. The problem with this approach is that the phase shifts predicted by our Hertzian model have the opposite sign to the phase shifts we observe. The reason for this discrepancy is that we have ignored adhesion in our model. Preliminary results from modeling that includes adhesion show that the phase shift changes sign and becomes consistent with our data. A description of this adhesive model will be presented in a future publication [32].

3. Conclusions

In-plane properties of materials can be observed using IC-AFM due to the tilt of the AFM cantilever which produces a small but significant in-plane component to the tip's motion. In the case of PDA monolayers, in-plane friction and shear deformation anisotropy leads to contrast in the IC-AFM phase image. The results can be explained using a simple model that incorporates Hertzian contact mechanics with in-plane dissipation. Adhesion must be added to the model in order to produce phase shifts of the proper sign.

A non-zero tilt ψ of the cantilever with respect to the sample normal is nearly universal in IC-AFM. Increasing the tilt angle would provide greater contrast in resolving in-plane properties, as demonstrated in the shear-force mode commonly used in near-field scanning optical microscopy [33]. Also, the local angle ψ will change due to local variations in sample topography, contributing to contrast in any phase image, even in the case of isotropic in-plane properties.

Acknowledgements

We thank J.P. Aimé and R. Garcia for useful discussions. We acknowledge funding from the NSF CAREER program, grant #DMR0094063 (MAE) and grant #CMS0134571 (RWC), the Research Corporation (MAE), and the NSF MRSEC program, grant #DMR0079983, and the University of Wisconsin-Madison. Some images in this paper were prepared using WSxM freeware from Nanotech Electronica.

References

[1] T.J. Ahrens, Mineral Physics & Crystallography: A Handbook of Physical Constants, American Geophysical Union, Washington, DC, 1995.
[2] B.L. Smith, T.E. Schlfferfi, M. Viani, J.B. Thompson, N.A. Frederick, J. Kindt, A. Belcher, G.D. Stucky, D.e. Morse, P.K. Hansma, Nature 399 (1999) 761.
[3] M. Liley, D. Gourdon, D. Stamou, U. Meseth, T.M. Fischer, C. Lautz, H. Stahlberg, H. Vogel, N.A. Burnham, C. Duschl, Science 280 (1998) 273.
[4] P.E. Sheehan, C.M. Lieber, Science 272 (1996) 1158.
[5] R.W. Carpick, D.Y. Sasaki, A.R. Burns, Trib. Lett. 7 (1999) 79.
[6] D.Y. Sasaki, R.W. Carpick, A.R. Burns, J. Colloid Interface Sci. 229 (2000) 490.
[7] H. Bluhm, U.D. Schwarz, K.P. Meyer, R. Wiesendanger, Appl. Phys. A 61 (1995) 525.
[8] R.M. Overney, H. Takano, M. Fujihira, W. Paulus, H. Ringsdorf, Phys. Rev. Lett. 72 (1994) 3546.
[9] R. Pearce, G.J. Vancso, Polymer 39 (1998) 6743.
[10] E. Amitay-Sadovsky, S.R. Cohen, H.D. Wagner, Appl. Phys. Lett. 74 (1999) 2966.
[11] A.R. Burns, R.W. Carpick, Appl. Phys. Lett. 78 (2001) 317.
[12] R.W. Carpick, M. Salmeron, Chem. Rev. 97 (1997) 1163.
[13] M.S. Marcus, R.W. Carpick, D.Y. Sasaki, M.A. Eriksson, Phys. Rev. Lett. 88 (2002) 226103.
[14] A. Lio, A. Reichert, D.J. Ahn, J.O. Nagy, M. Salmeron, D.H. Charych, Langmuir 13 (1997) 6524.
[15] J.P. Cleveland, B. Anczykowski, A.E. Schmid, V.B. Elings, Appl. Phys. Lett. 72 (1998) 2613.
[16] J. Tamayo, R. Garcia, Appl. Phys. Lett. 73 (1998) 2926.
[17] R.W. Carpick, D.F. Ogletree, M. Salmeron, Appl. Phys. Lett. 70 (1997) 1548.
[18] K.J. Wahl, S.V. Stepnowski, W.N. Unertl, Trib. Lett. 5 (1998) 103.
[19] N.A. Burnham, O.P. Behrend, F. Oulevey, G. Gremaud, P.-J. Gallo, D. Gourdon, E. Dupas, A.J. Kulik, H.M. Pollock, G.A.D. Briggs, Nanotechnology 8 (1997) 67.
[20] O.P. Behrend, L. Odoni, J.L. Loubet, N.A. Burnham, Appl. Phys. Lett. 75 (1999) 2551.
[21] O.P. Behrend, F. Oulevey, D. Gourdon, E. Dupas, A.J. Kulik, G. Gremaud, N.A. Burnham, Appl. Phys. A, Mater. Sci. Process. 66 (1998) S219.
[22] J.P. Spatz, S. Sheiko, M. Moller, R.G. Winkler, P. Reineker, O. Marti, Nanotechnology 6 (1995) 40.
[23] J. Tamayo, R. Garcia, Appl. Phys. Lett. 71 (1997) 2394.
[24] R. Garcia, A. San Paulo, Phys. Rev. B 60 (1999) 4961.
[25] D.F. Ogletree, R.W. Carpick, M. Salmeron, 2001, in preparation.
[26] L. Wang, Surf. Sci. 429 (1999) 178.
[27] H. Bielefeldt, F.J. Giessibl, Surf. Sci. 440 (1999) L863.
[28] L. Nony, R. Boisgard, J.P. Aimé, J. Chem. Phys. 111 (1999) 1615.
[29] F. Dubourg, J.P. Aimé, S. Marsaudon, R. Boisgard, P. Leclere, Eur. Phys. J. E 6 (2001) 49.
[30] U. Rabe, K. Janser, W. Arnold, Rev. Sci. Instrum. 67 (1996) 3281.
[31] R.S. Lakes, Viscoelastic Solids, CRC Press, Boca Raton, FL, 1999.
[32] M.S. Marcus, M.J. D'Amato, M.A. Eriksson, R.W. Carpick, in preparation.
[33] A.R. Burns, J.E. Houston, R.W. Carpick, T.A. Michalske, Langmuir 15 (1999) 2922.